Cellulose (2017) 24:1745–1758
DOI 10.1007/s10570-017-1219-8

ORIGINAL PAPER

Influence of high loading of cellulose nanocrystals in polyacrylonitrile composite films

Jeffrey Luo · Huibin Chang · Amir A. Bakhtiary Davijani · H. Clive Liu · Po-Hsiang Wang · Robert J. Moon · Satish Kumar

Received: 18 October 2016 / Accepted: 9 February 2017 / Published online: 14 February 2017

Abstract Polyacrylonitrile-co-methacrylic acid (PAN-co-MAA) and cellulose nanocrystal (CNC) composite films were produced with up to 40 wt% CNC loading through the solution casting method. The rheological properties of the solution/suspensions and the structural, optical, thermal, and mechanical properties of the resulting films were investigated. The viscosity of the composite suspensions increased with higher CNC loadings and with longer aging times. PAN-co-MAA/CNC films maintained a similar level of optical transparency even with up to 40 wt% CNC loading. The glass transition temperature (Tg) increased from 92 to 118 °C, and the composites had higher thermal stability below 350 °C compared to both neat PAN-co-MAA and neat CNC. The mechanical properties also increased with higher CNC loadings, elastic modulus increased from 2.2 to 3.7 GPa, tensile strength increased from 75 to 132 MPa, and the storage modulus increased from 3.9 to 10.5 GPa. Using the Kelly and Tyson model the interfacial shear strength between the PAN-co-MAA and CNC was calculated to be 27 MPa.

Keywords Cellulose nanocrystal · Nanocomposite · Polymer · Polyacrylonitrile

Introduction

Currently in the world there has been a huge drive to be more environmentally sustainable. This has led to the need to utilize more biorenewable resources. Cellulose nanocrystals (CNC) have been gaining significant interest as a reinforcement in polymer composites (Bondeson et al. 2006). CNC are formed by doing acid hydrolysis on the amorphous regions of cellulose which leaves the highly crystalline regions intact (Bondeson et al. 2006; Elazzouzi-Hafraoui et al. 2007). These rod shaped CNC have a diameter of 3–20 nm and a length of 50–500 nm depending on the source (Ebeling et al. 1999; Moon et al. 2011). CNC have an elastic modulus of 110–220 GPa, and a tensile strength of 7.5–7.7 GPa (Moon et al. 2011). Along with its high surface area, biodegradability, biorenewability, and low toxicity, CNC have been shown to

Electronic supplementary material The online version of this article (doi:10.1007/s10570-017-1219-8) contains supplementary material, which is available to authorized users.

J. Luo · H. Chang · A. A. Bakhtiary Davijani · H. C. Liu · P.-H. Wang · R. J. Moon · S. Kumar (✉)
School of Materials Science and Engineering, Georgia Institute of Technology, Atlanta, GA 30332, USA
e-mail: Satish.Kumar@mse.gatech.edu

J. Luo · H. Chang · H. C. Liu · R. J. Moon · S. Kumar
Renewable Bioproducts Institute, Georgia Institute of Technology, Atlanta, GA, USA

R. J. Moon
The Forest Products Laboratory, US Forest Service, Madison, WI 53726, USA

be an effective reinforcement in polymer composites (Habibi et al. 2010; Lin and Dufresne 2014; Siqueira et al. 2010).

Many studies have already been done on CNC composite films with many different types of polymer matrices including polymethyl methacrylate (PMMA) (Kiziltas et al. 2015), polyvinyl alcohol (PVA) (Fortunati et al. 2013; Rescignano et al. 2014; Roohani et al. 2008; Xu et al. 2013b), polylactic acid (PLA) (Kamal and Khoshkava 2015; Lin et al. 2011), polyvinylidene fluoride (PVDF) (Bai et al. 2012), polyvinyl chloride (PVC) (Chazeau et al. 2000), polypropylene (PP) (Ljungberg et al. 2006), poly(3-hydroxybutyrate-co-3-hydroxyvalerate) (PHBV) (Jiang et al. 2008; Yu et al. 2012; Yu et al. 2011), acrylonitrile butadine styrene (ABS) (Ma et al. 2015), polyurethane (Liu et al. 2015; Marcovich et al. 2006), epoxy (Girouard et al. 2015; Xu et al. 2013a), starch (Agustin et al. 2013), and chitosan (Khan et al. 2012). The incorporation of CNC into the polymer matrix can increase the elastic modulus, tensile strength, storage modulus, glass transition temperature (Tg), and thermal stability. In previous studies on films the incorporation of CNC increased the elastic modulus 23–50% in PVA (Fortunati et al. 2013; Rescignano et al. 2014; Roohani et al. 2008), 42% in PLA (Lin et al. 2011), 115–250% in PHBV (Jiang et al. 2008; Yu et al. 2012), 35% in ABS (Ma et al. 2015), 69–144% in polyurethane (Liu et al. 2015; Marcovich et al. 2006), 64% in epoxy (Xu et al. 2013a), 34% in starch (Agustin et al. 2013), 87% in chitosan (Khan et al. 2012), and an increase was also seen in PVC (Chazeau et al. 2000). The tensile strength increased 25–32% in PVA (Roohani et al. 2008; Xu et al. 2013b), 61% in PLA (Lin et al. 2011), 35% in PVDF (Bai et al. 2012), 42% in PP (Ljungberg et al. 2006), 85–149% in PHBV (Jiang et al. 2008; Yu et al. 2012), 16% in ABS (Ma et al. 2015), 28% in polyurethane (Liu et al. 2015), 50–77% in epoxy (Girouard et al. 2015; Xu et al. 2013a), 56% in starch (Agustin et al. 2013), and an increase in PVC (Chazeau et al. 2000) was also seen. The values of the elastic modulus and tensile strength of the neat polymer matrices and the CNC composites can be found in supplementary information Table S1. Storage modulus increased 20% in PLA (Kamal and Khoshkava 2015), 20% increase in PHBV (Jiang et al. 2008), 49% increase in epoxy (Girouard et al. 2015), and increases were also seen in PVA (Roohani et al. 2008), PP (Ljungberg et al. 2006), and polyurethane (Liu et al. 2015). The Tg increased 5 °C in PHBV (Jiang et al. 2008), and 2 °C in polyurethane (Liu et al. 2015). Thermal stability also increased in PMMA (Kiziltas et al. 2015), PHBV (Yu et al. 2012), and polyurethane (Liu et al. 2015).

Polyacrylonitrile (PAN) is the predominant precursor for carbon fiber, and it currently accounts for more than 90% of the industrially produced carbon fiber (Rahaman et al. 2007). With the incorporation of CNC into PAN, more biorenewable carbon materials and carbon fiber can be produced. For the production of carbon fiber homopolymer PAN is not used due to the narrow temperature range of the exothermic reaction during the stabilization process. This reaction is very rapid and releases large amounts of heat, which locally damages the fiber and lowers the mechanical properties of the carbon fiber produced. To counter this problem acrylonitrile is usually copolymerized with another monomer, two examples are methyacrylic acid (MAA) and itaconic acid (IA). These copolymers broaden the temperature range over which the exothermic reaction occurs, extending the time period over which the heat of reaction is released, which subsequently minimizes damage to the fiber (Park 2015).

High aspect ratio reinforcements have been previously incorporated into polyacrylonitrile-co-methacrylic acid (PAN-co-MAA) to improve properties. There has been a study on PAN-co-MAA films with a loading of 20 wt% single wall carbon nanotubes (SWNT) that increased the elastic modulus from 2.7 to 9.3 GPa, tensile strength from 57 to 102 MPa, and Tg from 88 to 108 °C (Guo et al. 2010). Previously PAN-co-MAA/CNC fibers with a loading of 10 wt% CNC were made, which showed an increased elastic modulus from 14.5 to 19.6 GPa, tensile strength from 624 to 709 MPa, and Tg from 93 to 103 °C (Chang et al. 2015). However, the role of higher CNC loading into PAN-co-MAA has not been reported.

In the current study PAN-co-MAA/CNC films were produced with loadings up to 40 wt % CNC through the solution casting method, and the structural, optical, mechanical, and thermal properties were investigated. The rheology of the PAN-co-MAA solution and the composite suspensions used to make the films were also investigated. This advancement in understanding of the role higher CNC loadings have on rheological, mechanical, and thermal properties, can be subsequently applied to PAN-co-MAA/CNC fiber processing and the ensuing use as a precursor for a more biorenewable carbon fiber.

Table 1 Solid content of the solution and suspensions used to make the films, and the volume percent CNC in these suspensions

Sample	Neat PAN-co-MAA	CNC-5	CNC-10	CNC-20	CNC-30	CNC-40
Solid content[a] (wt%)	4.0	3.8	4.0	3.9	4.1	4.1
Volume percent CNC in suspension	0	0.1	0.2	0.5	0.7	1.0

[a] Solid content (polymer and CNC) of the solution and suspensions used to make the films and rheology study, solid content was measured with thermal gravimetric analysis under nitrogen atmosphere at 180 °C

Experimental

Materials

Polyacrylonitrile-co-methacrylic acid (PAN-co-MAA; 4 wt% of MAA content, viscosity average molecular weight: 2.47×10^5 g/mol) was obtained from Exlan Co., Japan, and will be referred to as PAN-co-MAA powder. Freeze dried CNC (lot# 2012-FPL-CNC-48/051) produced by USDA Forest Service - Forest Products Laboratory (FPL), were obtained from the University of Maine, US, and will be referred to as freeze dried CNC. The dimensions of these CNC were previously measured to be approximately 6.3 nm in diameter and 153 nm in length (Chang et al. 2016). Dimethylformamide (DMF) was obtained from Sigma-Aldrich co. and was distilled before use.

Solution/suspension preparation

The PAN-co-MAA solution and PAN-co-MAA/CNC suspensions were targeted to have a solid content of 3.7 wt% in DMF. Six different solution/suspensions were made with 0, 5, 10, 20, 30, and 40 wt% CNC with respect to the weight of the polymer; these samples will be referred to as neat PAN-co-MAA, CNC-5, CNC-10, CNC-20, CNC-30, and CNC-40, respectively. To make one of the suspensions the desired amount of freeze dried CNC (depending on the final CNC content) were dispersed in 100 ml of DMF by a bath sonicator (Branson 3510R-MT, 100 W, 42 kHz) for 24 h. This CNC/DMF suspension was then combined with PAN-co-MAA powder in a glass reactor and mechanically mixed at 200 rpm at 70 °C for 3–4 h. The same procedure was followed to make the neat PAN-co-MAA solution except the first step of dispersing the freeze dried CNC in DMF was not used. The air bubbles were removed from the solution/suspension in a vacuum oven at 70 °C for 5 min. Due to the solution/suspension preparation process the final solid content ended up higher than 3.7 wt% and the measured solid content of each solution/suspension is given in Table 1. A 100 wt% CNC suspension was also made by dispersing the freeze dried CNC in deionized (DI) water to make a 1 wt% solid content suspension, and will be referred to as neat CNC.

Film preparation

Neat CNC films were made by solution casting into a polystyrene petri dish, and dried in an oven at 70 °C for 2 days. This film was used only in thermogravimetric analysis, differential scanning calorimetry, and wide angle x-ray diffraction. The neat PAN-co-MAA and PAN-co-MAA/CNC films were made by solution casting (4 h after the solution/suspension has been made) into a glass mold, and dried in an oven at 70 °C for at least 4 h. The neat PAN-co-MAA and PAN-co-MAA/CNC films were removed from the oven, cooled down to room temperature, then submerged in deionized (DI) water for 30 min, and removed from the glass mold. This film was then placed between two glass plates and a normal stress of around 80 Pa was applied to the film. This assembly was placed in a drying oven at 70 °C for 12 h to remove residual stress that would otherwise cause the film to curl.

To make tensile and DMA specimens the films were rehydrated by submerging in DI water until they could be cut without cracking ($\sim$1 h). These films were then cut into rectangular strips using a cutting apparatus incorporating a razor blade. These film strips were then placed between the two glass plates and a normal stress of around 80 Pa was applied to the strips. This assembly was placed in a drying oven at 70 °C for 12 h. The strips were then taped onto paper tabs and further dried under vacuum at 40 °C for 24 h. The samples were stored in a desiccator until testing to help minimize moisture uptake to help mitigate moisture induced effects on the mechanical properties

Table 2 Thermal and mechanical properties of the films. Also the film dimensions and the volume percent CNC in the films

Sample	Neat PAN-co-MAA	CNC-5	CNC-10	CNC-20	CNC-30	CNC-40
Vol% CNC in films	0	3.8	7.6	15.7	24.2	33.2
Film thickness[a] (μm)	93 ± 5	104 ± 4	117 ± 9	105 ± 1	115 ± 5	104 ± 3
Elastic modulus (GPa)	2.2 ± 0.1	2.4 ± 0.1	2.4 ± 0.1	3.0 ± 0.1	3.2 ± 0.1	3.7 ± 0.1
Tensile strength (MPa)	75 ± 3	84 ± 3	91 ± 4	97 ± 9	116 ± 6	132 ± 9
Strain at break (%)	27.3 ± 16.4	9.9 ± 3.1	5.3 ± 0.6	4.0 ± 0.8	4.3 ± 0.3	4.2 ± 0.4
Storage modulus at 35 °C (GPa)	3.9	4.4	5.3	7.3	9.0	10.5
Tg (°C)	92	96	97	106	118	N/A

[a] Film thickness of the samples used for tensile test and dynamical mechanical analysis

of the films. The thickness of these samples can be found in Table 2.

Characterization

Rheological measurements were performed on an ARES rheometer (Rheometric Scientific, Co.). The testing was done at room temperature, with 50 mm parallel plates, and a gap size of 1 mm. To prevent evaporation of solvent and absorption of water during testing, a layer of silicone oil was applied to the exposed sample surface around the sides of the parallel plates. The linear viscoelastic region (LVR) was determined for each sample by running a strain sweep test at an oscillatory frequency, ω, of 5, 10, and 100 rad/s. A frequency sweep was done from 5 to 100 rad/s in the LVR for each sample, and then the same sample between the plates was immediately ran again for a second run with the same parameters. By comparing the first and second runs of the frequency sweep it is possible to assess if solvent evaporation, water adsorption, or if a breakdown of a percolation network took place during the test. The bulk solution/suspension samples were kept in vials, sealed with Teflon tape and stored in a dark cabinet at room temperature to help prevent evaporation of solvent, and to prevent degradation of the polymer due to light for the rheology aging study, since PAN is known to degrade when exposed to ultraviolet radiation (Aggour and Aziz 2000). For the rheology aging study each sample was tested at 4 h, 4, 14, 30, and 90 days after the solution/suspension has been made. The aged solution/suspensions solid content was checked with a TGA and it was determined that there was no change in the solid content over the 90 day period.

Fourier transform infrared spectroscopy (FTIR) was done on a Magna 560 FTIR (Nicolet Instruments) to study the interactions between the PAN-co-MAA and CNC. The tests were done on neat PAN-co-MAA and composite films, but the pure CNC spectra was done with the freeze dried CNC powder and KBr due to the difficulties of making a thin enough film. The scan range was 400–4000 cm^{-1} with resolution of 0.5 cm^{-1}. Wide-angle X-ray diffraction (WAXD) was done with Rigaku MicroMax-002 (CuK_{α}, $\lambda = 0.1542$ nm) and a Rigaku R-axis IV++ detector. MDI Jade 9 software was used to analyze the WAXD pattern.

Ultraviolet–Visible (UV–Vis) spectroscopy was done to determine the transparency of the films; measurements were done on a Lambda 35 (PerkinElmer Co.). The scan was done over a range of 200–800 nm with a scan speed of 480 nm/min with a resolution of 1 nm. To assess the degree of micron sized CNC agglomerations in the films, polarized light microscopy (Leica DM2500 P, Leica Microsystems) was used to determine if there were regions of birefringence, which can be caused by agglomeration of CNC (Girouard et al. 2015). Films were observed in transmission mode under cross polarizers with an objective of 4×. To further characterize dispersion the fracture surface of the films after tensile testing were sputtered with gold and observed by scanning electron microscope (Zeiss Ultra60 FE-SEM).

Thermal stability and degradation were investigated with thermogravimetric analysis (TGA) with TA

instruments Q500. Samples were dried under vacuum at 70 °C for 24 h and stored in a desiccator until they were tested. These samples were tested within 5 min from being removed from the desiccator. Samples were tested under both air and nitrogen atmosphere with the sample size ranging from 5 to 6 mg. The samples were heated from 50 to 795 °C at a heating rate of 10 °C/min. Differential scanning calorimetry (DSC) was ran on TA instrument Q100. Sample sizes of ~3 mg were used in standard aluminum pans. Samples were heated from 50 to 300 °C at 10 °C/min in air.

Dynamic mechanical analysis (DMA) and tensile testing were completed using a RSA III solids analyzer (Rheometric Scientific Co.). The samples tested were rectangular strips having a gauge length of 12.7 mm, width of ≈2.2–2.5 mm, and an average thickness of ~100 μm (see Table 2). The width of the each specimen was measured in nine different areas with an optical microscope (Leica DM2500 P, Leica Microsystems) and ImageJ, while the thickness was measured with a digital micrometer (Mitutoyo 331-361 Type B) in three different areas. To maintain consistency if the variation of width and thickness were greater than 100 and 10 μm, respectively, the samples were not used. Dynamic mechanical tests were conducted at a frequency of 1 Hz, 0.1% dynamic strain, over a temperature range of 35–170 °C with a heating rate of 1 °C/min. Tensile tests were completed at room temperature at a strain rate of 5%/min. Tensile testing continued until there were at least five samples that did not break at the grip for each different composition. For the specimens that broke at the grip, the results were not used due to the possibility that the fracture occurred because of stress concentration caused by the grips.

Results and discussion

Rheology of PAN-co-MAA/CNC suspensions

The effect of frequency (up to 100 rad/s), CNC loading (up to 1 vol%), and aging time (4 h, 4, 14, 30, and 90 days) on the complex viscosity of PAN-co-MAA/CNC suspensions were measured (frequency sweep plots for all samples are shown in Fig. S1). The frequency sweep plots of the solution/suspensions used to cast the films (4 h age time) is shown in Fig. 1 (left). The first and second runs for all the samples tested at each age were similar, indicating that there was little to no solvent evaporation or water absorption during the test. This also indicates that the structure within the suspension is consistent between the runs. The comparison between the first and second runs can be seen in Fig S2. The neat PAN-co-MAA solution had a Newtonian behavior up to 100 rad/s, while the incorporation of CNC lead to suspensions having a shear thinning behavior. The mechanism causing the shear thinning behavior is likely due to the alignment of the rod-like CNC during shear, which has been observed in other CNC systems (Kamal and Khoshkava 2015; Marcovich et al. 2006) and other high aspect ratio particle systems, such as carbon nanotubes and titanate nanotubes (Chen et al. 2009; Karpushkin et al. 2014). Overall, there is a general trend of increasing viscosity with increasing CNC loading over all frequencies and for all aging times (Fig. S1). For the aging times of 4 to 90 days this trend was observed, however at the 4 h aging time the CNC-20 and CNC-40 had viscosities a bit lower than expected. The increase in viscosity with increasing CNC loading is expected at low shear rates because the CNC behaves like a filler in the suspension.

The effect of aging time (up to 90 days) and CNC loading (up to 1 vol%) on complex viscosity (at 5 rad/s) is shown in Fig. 1 (right). All of the PAN-co-MAA/CNC suspensions were observed to have increasing viscosity with increasing aging time, in contrast, the viscosity of the neat PAN-co-MAA solution was minimally affected or had a slight decrease in viscosity. There was larger increase in viscosity over time with higher CNC loading, but the extent of change effectively stopped after 2 weeks for all samples. The increase in viscosity of the suspension with aging time is considered to result from polymer–filler interaction, as opposed to the formation of a percolated CNC network. Polymer adsorption onto fillers have been previously reported to increase the viscosity of a system with time (Anderson and Zukoski 2009; Huang et al. 2011). This scenario may be possible with PAN-co-MAA adsorbing onto the CNC over time, though we do not provide any direct evidence for this in this study. In contrast, the study by Derakhshandeh et al. (2013) showed that CNC network formation in neat a CNC suspension (10 wt% solid) can increase viscosity of the system with time. In our system the increase in viscosity with time

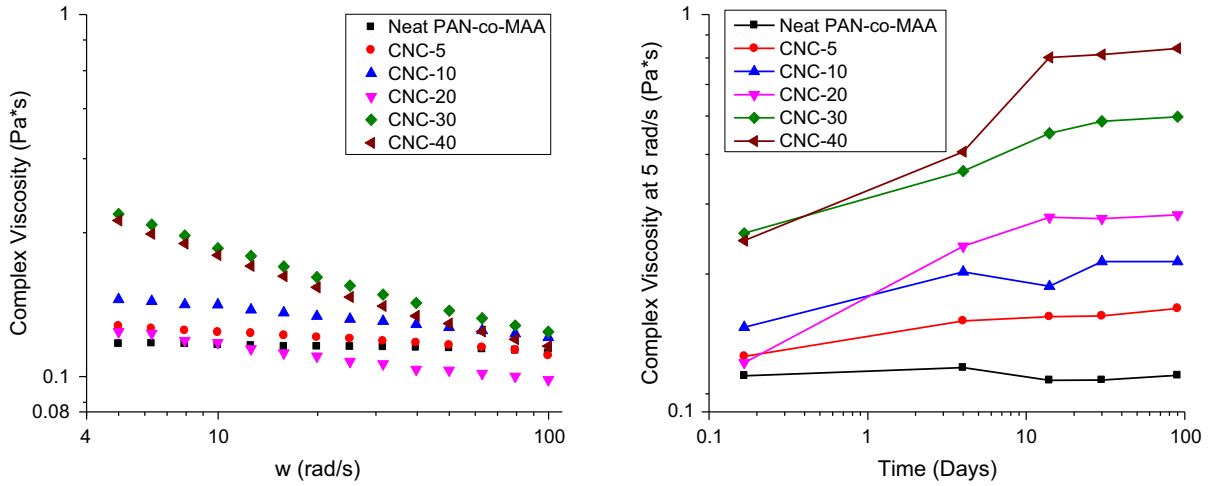

Fig. 1 Complex viscosities of solution/suspensions (*left*) 4 h after being made (frequency sweeps from 5 to 100 rad/s), and (*right*) over a 3 months period at 5 rad/s. Solid contents of these solution/suspensions can be found in Table 1

is not believed to result from the formation of a CNC network structure for several reasons. First, testing was done in the linear viscoelastic region, determined in lead up experiments, so the structure within the suspension is recovering during the testing. Secondly, the suspensions are shear thinning indicating alignment of CNC in the shear direction. Also with the viscosity curves of the first and second run of the same sample being very similar, it indicates no change in structure within the suspension that was not recovered between the first and second run. If the increased viscosity was due to percolation the first and second runs should be different as there would be insufficient time for the percolation network to reform, since the second run was ran immediately after the first run while the increase in viscosity was developed over a longer period of time (hours to months). Finally, the vol% of CNCs used in the current study was at or below 1 vol%, which is below the percolation threshold of ~2.9 vol% for the aspect ratio of the CNCs used in our system (Siqueira et al. 2010) (see percolation threshold calculations in supporting documentation).

Chemical interaction and structure

FTIR results for the film are given in Fig. 2. The characteristic peak for PAN is the peak at 2243–2240 cm^{-1} belonging to the CN (nitrile), and the peak at 1733–1723 cm^{-1} belongs to the carbonyl group in the methacrylic acid (MAA). The peaks at 2940–2930, 2850, 1450, 1360, and 1050 cm^{-1} belong to aliphatic CH, CH_2, and CH_3 in the PAN or MAA (Loginova et al. 2016). For the CNC the characteristics peaks at 3490–3175 and 1649–1634 cm^{-1} belongs to OH (hydroxyl), 2900 and 1382–1375 cm^{-1} belongs to CH, and the peaks at 1430–1420 and 1317 cm^{-1} belong to CH_2 (Kumar et al. 2014). There is no observable interaction from the FTIR between the CNC and the PAN as determined from the lack of shift of the CN peak, and no observable new peaks developing. There was an observed shift of the peak related to the carbonyl group of MAA, the peaks shifted from 1724 cm^{-1} in neat PAN-co-MAA to 1734 cm^{-1} in the CNC-10 film and stayed around 1734 cm^{-1} at higher CNC loadings (Fig. 2 right). This indicates that there is interaction between the CNC and the MAA copolymerized with the PAN. There have been previous studies that showed interaction between carbonyl and hydroxyl groups (Jiang et al. 2008; Schuster 1969; Yu et al. 2012).

The incorporation of CNC into the PAN-co-MAA matrix did not have significant influence on the percent crystallinity of the PAN-co-MAA as estimated by WAXD. The procedure and results can be found in the supplementary information (Fig. S8, Fig. S9, and Fig. S10).

Optical properties

The addition of up to 40 wt% CNC loading did not have a detrimental effect on the optical transparency

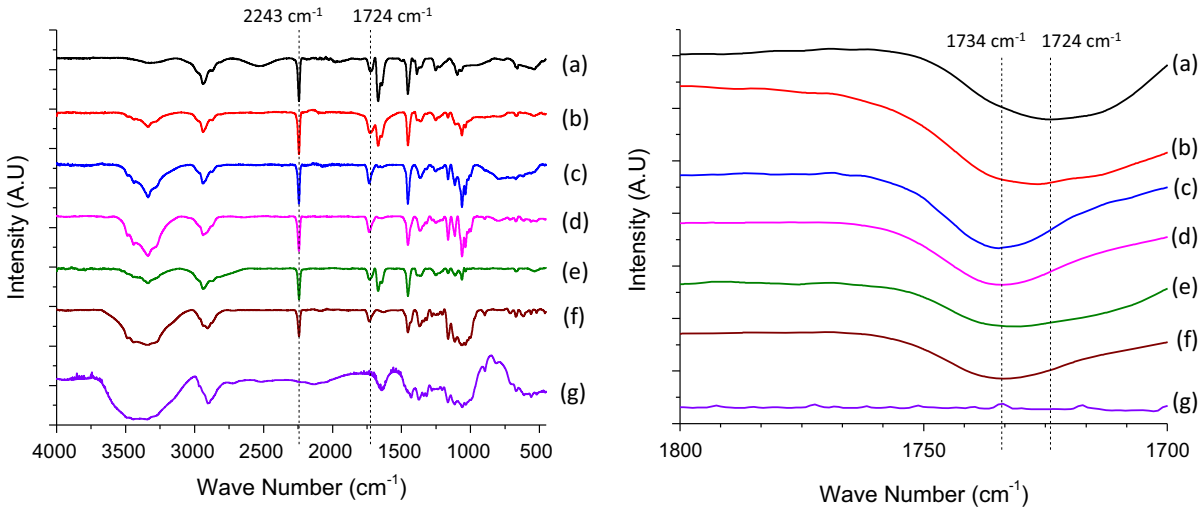

Fig. 2 FTIR spectra of films (*left*) FTIR full spectrum, (*right*) FTIR spectrum from 1800 to 1700 cm^{-1} to display carbonyl peak shift with the addition of CNC. *a* neat PAN-co-MAA, *b* CNC-5, *c* CNC-10, *d* CNC-20, *e* CNC-30, *f* CNC-40, *g* freeze dried CNC

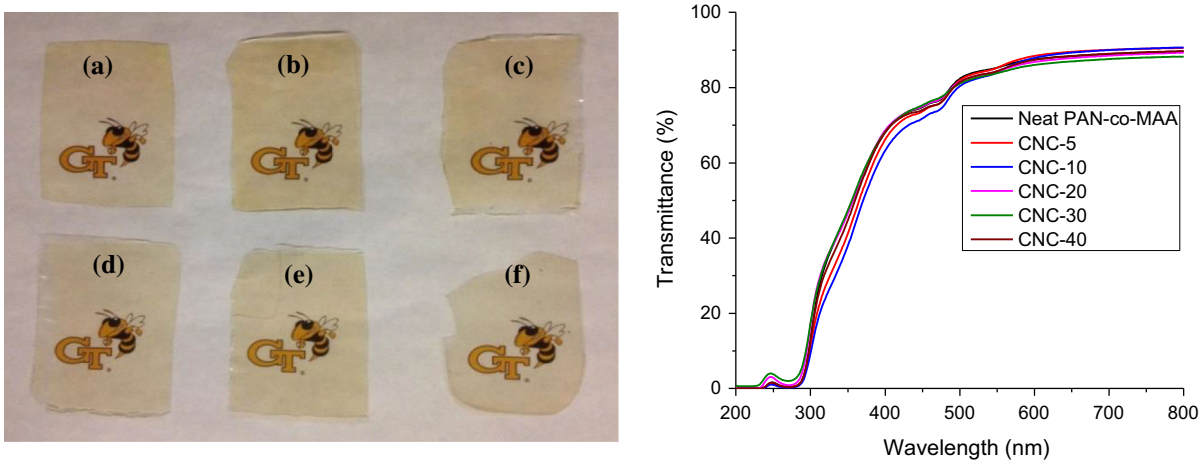

Fig. 3 (*Left*) Optical images of films displaying transparency *a* neat PAN-co-MAA, *b* CNC-5, *c* CNC-10, *d* CNC-20, *e* CNC-30, *f* CNC-40. (*Right*) UV–Vis spectra showing small differences in transmittance of the films (all thicknesses comparable)

and color, which can be seen in Fig. 3. The films look homogenous at the macro scale. To estimate the degree of CNC agglomeration at a finer length scale (e.g. micron-sized agglomerates), polarized light microscopy was used. Differences in birefringence between the polymer matrix and agglomerated CNC domains have been used to qualitatively assess the extent of CNC agglomeration within composites (Girouard et al. 2015). In our system, there is little observable birefringence within the majority of the neat PAN-co-MAA and PAN-co-MAA/CNC films (Fig. S3), suggesting a limited amount of micron sized CNC agglomeration. Incidentally, there were isolated regions of increased birefringence (Fig. S4), these areas were considered worst-case-scenarios, and were not representative of the whole film. With this in mind, and considering the study by Girouard et al. (2015) that showed extensive birefringence at 5 wt % CNC loading, which is considerably lower than the loadings used in the current study (up to 40 wt%), it can be considered that the PAN-co-MAA/CNC composite films had a low degree of micron sized CNC agglomeration. In support of this, fracture surfaces of PAN-co-MAA/CNC composite films do not show fracture

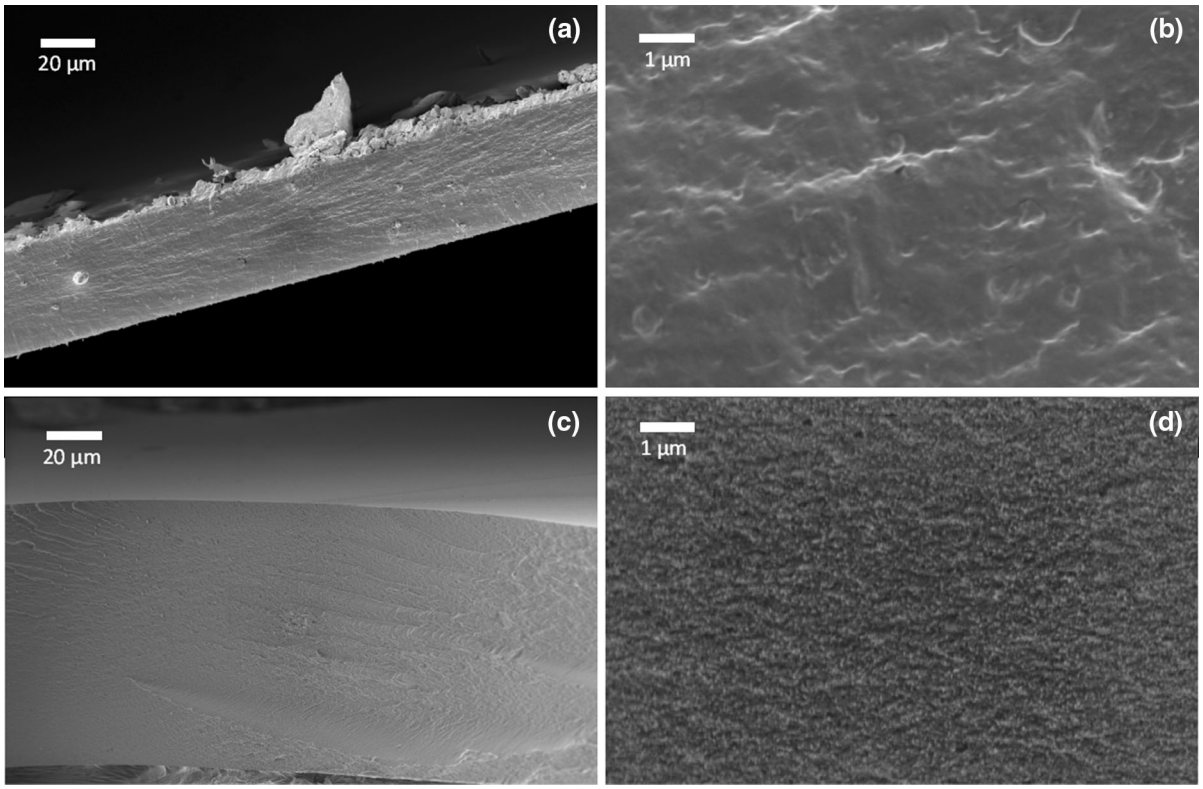

Fig. 4 SEM images of the fracture surfaces of films after tensile testing **a** neat PAN-co-MAA **b** neat PAN-co-MAA **c** CNC-40, and **d** CNC-40. No apparent aggregations are seen in the CNC-40 film. The neat PAN-co-MAA is significantly thinner in these images because of the large amount plastic deformation during tensile testing, compared to the CNC-40 film

features that would be indicative of micron sized agglomerates (Fig. 4).

Thermal properties

Thermal stability studies on the films with similar thickness were conducted using TGA in both air and nitrogen, and the results of these tests are shown in Fig. 5. The nanocomposites had better thermal stability (e.g. lower weight loss) up to ≈350–375 °C depending on the CNC loading compared to the neat PAN-co-MAA film in both air and nitrogen. This is surprising because the neat CNC film has much lower thermal stability compared to the neat PAN-co-MAA film at these temperatures. This unusual behavior of CNC-polymer composites having better thermal stability than both the neat polymer and the neat CNC have been reported before (Liu et al. 2015; Yu et al. 2012).

An unexpected result is the residue yield after heating up the films up to 795 °C in nitrogen atmosphere. The neat PAN-co-MAA and all the nanocomposite films had a residue yield around 50 wt%, while the neat CNC film had a residue yield of around 30 wt% as seen in Fig. 5. This means that the degradation of the composites does not follow the rule of mixtures, and indicates chemical interaction between the CNC and PAN-co-MAA as the composite undergoes heating. A graph of the experimental and rule of mixture residue yield can be seen in Fig. 5 (bottom). The experimental and rule of mixture degradation graph of CNC-40 in both air and nitrogen can be seen in Fig. S5.

The tan δ peak is the Tg of the system (Fig. 6), and it was seen that it increased with increasing CNC content. The Tg for the neat PAN-co-MAA was 92 °C and increased to 118 °C for CNC-30. Tg for CNC-40 could not be determined due to no observable peak. The Tg was also determined by DSC and a similar trend of increasing Tg with increasing CNC loading was seen and can be seen in Table S2 and Fig S7. The tan δ peak height also decreased from 0.27 for neat PAN-co-MAA to 0.11 for the CNC-30. A lower tan δ

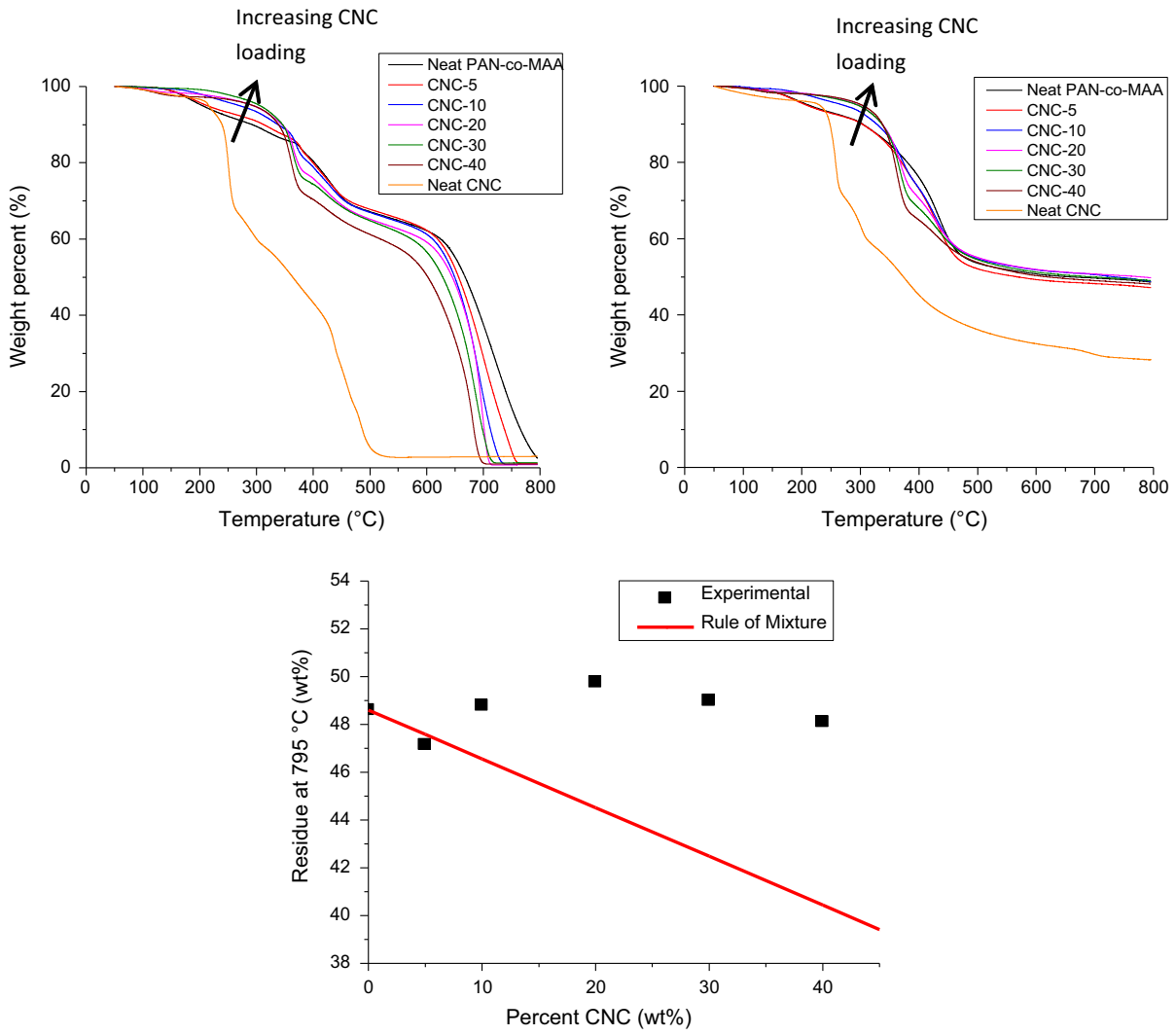

Fig. 5 TGA results of the films at a heating rate of 10 °C/min (*top left*) in air 50–795 °C, (*top right*) in N_2 50–795 °C, (*bottom*) experimental and rule of mixture residue (wt%) of the films from the rule of mixtures at 795 °C in N_2

indicates lower chain mobility, this is likely due to the long rigid rod-like CNCs physically constraining polymer movement.

Mechanical properties

The storage modulus of the films measured at a frequency of 1 Hz are given in Fig. 6 and Table 2. There was a trend of increasing storage modulus with increasing CNC loading. At 35 °C the storage modulus for the neat PAN-co-MAA and CNC-40 film was 3.9 and 10.5 GPa, respectively. With higher CNC loading the reduction in the storage modulus with increasing temperature was decreased. This is likely due to the filler and polymer interaction, and also possibly a CNC percolation network within the films. The CNC percolation network is less sensitive to temperature compared to the PAN-co-MAA matrix. At 20 wt% and higher CNC loadings there is a large increase in the storage modulus at the plateau temperature indicating that a CNC percolation network has possibly formed. The storage modulus was also seen to increase in some of the films after the plateau temperature, this is due to the PAN-co-MAA undergoing cyclization. The onset of this increase in storage modulus increased with increasing CNC

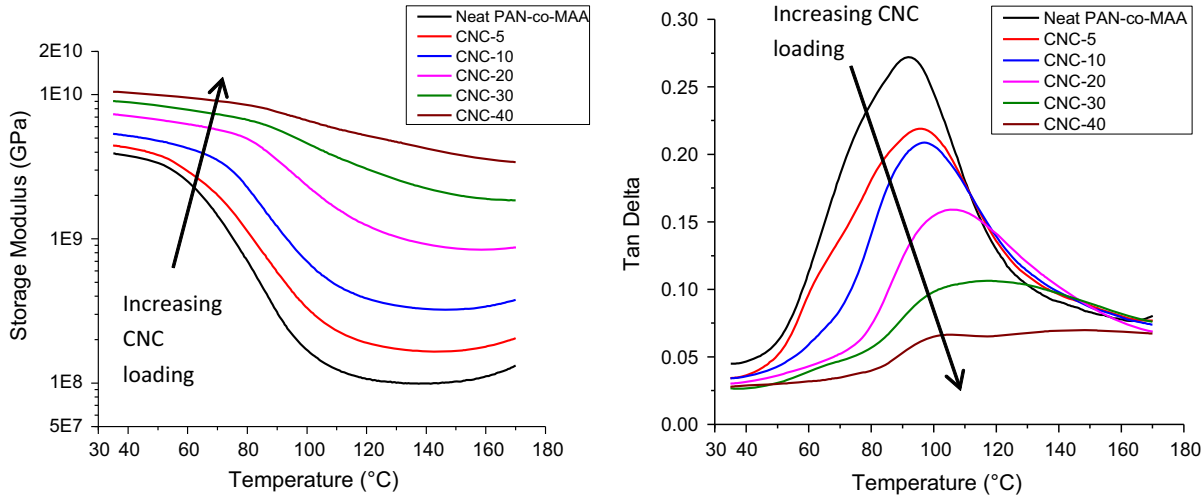

Fig. 6 Dynamical mechanical analysis results of films at a frequency of 1 Hz (*left*) Storage Modulus, (*right*) Tan Delta

loading, likewise the cyclization onset temperature also increased with increasing CNC loading (Table S2 and Fig S7).

The tensile testing results are given in Table 2. There was a trend of increasing elastic modulus and tensile strength with increasing CNC loading. There was also a trend of decreasing strain at break with increasing CNC loading up to 20 wt% CNC, but above 20 wt% CNC loading there was not much change. The comparable strain at break at 20 wt% CNC and above is considered to result from a similar failure mechanism associated with the breaking of a percolated CNC network structure. In partial support for this, the storage modulus data at 20 wt% CNC and above indicated that a percolation network had formed. Comparing the neat PAN-co-MAA to the CNC-40 film, the elastic modulus increased from 2.2 to 3.7 GPa, the tensile strength increased from 75 to 132 MPa, while the strain a break decreased from 27.3 to 4.2%, respectively. These changes in properties due to the addition of CNC may be a result from several mechanisms, such as increased crystallinity of PAN-co-MAA, PAN-co-MAA/CNC interfacial interactions, CNCs acting as a reinforcement phase, and/or the formation of a CNC percolation network. WAXD results indicate that the increase in mechanical properties was not due to higher crystallinity of the PAN-co-MAA (see description in supporting information).

The role of the PAN-co-MAA/CNC interface on properties was considered by assessing the interfacial shear strength, which would give an indication of the load transfer between the matrix phase and the CNC reinforcement phase. The equation for the critical interfacial shear strength needed between the CNC and the matrix for the tensile strength of the CNC to be fully utilized can be found in Eq. 1. Where τ_c, σ_f, D, and L

$$\tau_c = \frac{\sigma_f D}{2L} \tag{1}$$

are the critical shear strength of the interface, tensile strength of reinforcement (e.g. CNC), diameter of reinforcement, and length of reinforcement, respectively (Eichhorn 2011). Using a CNC length of 153 nm, diameter of 6.3 nm, and a tensile strength of 7.5 GPa (Moon et al. 2011) the critical shear strength of the interface would need to be 154 MPa to fully utilize the tensile strength of the CNC. The interfacial shear strength between various polymers and various types of reinforcements typically does not exceed 80 MPa (Cho et al. 2009; Haspel et al. 2015; Newcomb et al. 2014; Swentek and Wood 2013; Zafeiropoulos 2011).

To estimate the critical reinforcement length needed to fully utilize the tensile strength of the CNC reinforcement for our system, the Thomason modified (Thomason et al. 1996) Kelly and Tyson (1965) equation for randomly oriented short fiber composites was used. Assuming all the CNC are the same length and diameter, and individually dispersed, the modified equation for tensile strength of the composite, σ_c, is given in Eq. 2. where η_0, ϕ_1, σ_f, σ_m, L and L_c are the orientation factor of reinforcement,

$$\sigma_c = \eta_0 \frac{\phi_1 \sigma_f L}{2L_c} + (1 - \phi_1)\sigma_m \quad (2)$$

volume fraction of reinforcement, tensile strength of reinforcement, tensile strength of matrix, length of reinforcement, and critical reinforcement length, respectively. For a 2-D randomly oriented composite the η_0 can be assumed to be 3/8 (Li et al. 2016; Thomason et al. 1996). The elastic modulus of the matrix used was the elastic modulus of the neat PAN-co-MAA film which was 2.2 GPa. Solving the equation with the experimental data gave a critical reinforcement length of 876 nm (Fig. S6), and plugging this value back into Eq. 1 gave an interfacial shear strength of 27 MPa. This should only be considered as an estimate as the actual interfacial shear strength might either be lower due to the possible formation of a CNC percolation network within the films, or could be higher if the CNCs are not individually dispersed in the matrix. Combining these results with the measured average CNC length used in the current study, 153 nm, it suggests that it is not possible to fully utilize the tensile strength of the CNC in the PAN-co-MAA composites.

To estimate the effectiveness of CNC in stiffening PAN-co-MAA the Cox-Krenchel model (Eq. 3) for short fiber composites was used. The Cox-Krenchel model assumes the reinforcement and matrix respond elastically, no axial loading on the reinforcement ends, and that there is a perfect matrix/reinforcement interface (Lee et al. 2014). The terms η_0, η_L, E_c, E_f, E_m, and ϕ_1 represent orientation factor of reinforcement, reinforcement stress transfer efficiency, elastic modulus of the composite, effective elastic modulus of reinforcement, elastic modulus of matrix, and volume fraction of reinforcement, respectively. The η_L (reinforcement stress transfer efficiency) can be calculated with Eq. 4 with the variable β being equal to Eq. 5. The terms ν_m, L, D, and P_f represents Poisson ratio of the matrix, length of reinforcement, diameter of reinforcement, and packing factor of the reinforcement (Cox 1952; Krenchel 1964).

$$E_c = \eta_0 \eta_L \phi_1 E_f + (1 - \phi_1)E_m \quad (3)$$

$$\eta_L = 1 - \frac{\tanh\left(\frac{\beta L}{2}\right)}{\frac{\beta L}{2}} \quad (4)$$

$$\beta = \frac{2}{D}\sqrt{\frac{E_m}{(1+\nu_m)E_f \ln\left(\sqrt{\frac{P_f}{\phi_1}}\right)}} \quad (5)$$

The length and diameter of the reinforcement used was 153 and 6.3 nm, respectively. The square packing factor, $\pi/4$, is often used for CNC composites, and was used for our calculations (Battegazzore et al. 2016; Maqsood et al. 2016; Visakh et al. 2012). The Poisson ratio of the PAN matrix used was 0.07 (Ozkul et al. 1993).

Using Eqs. (3)–(5) and the methods of least squares, solving for E_f the effective elastic modulus of the CNC was calculated. Fitting the data gave a CNC effective elastic modulus of 19 GPa (Fig. 7). This is much lower than the experimental and theoretical elastic modulus of CNC, which is 110–220 GPa, suggesting that the CNCs are underutilized in stiffening PAN-co-MAA. Considered here are two plausible mechanisms for why the CNC effective modulus was lower than the experimental and theoretical CNC modulus, (i) CNC agglomeration within the matrix, and (ii) less than 100% efficient stress transfer across the CNC matrix interface. CNC agglomeration is not desirable as it effectively results in a larger sized reinforcement particle, which significantly lowers CNC/matrix surface area, and has diminished mechanical properties as compared to individual CNC. Using the Cox-Krenchel equations, larger sized CNC agglomerate should lead to lower reinforcement efficiency. The low extent of CNC agglomeration in the PAN-co-MAA/CNC films qualitatively assessed from optical and polarized

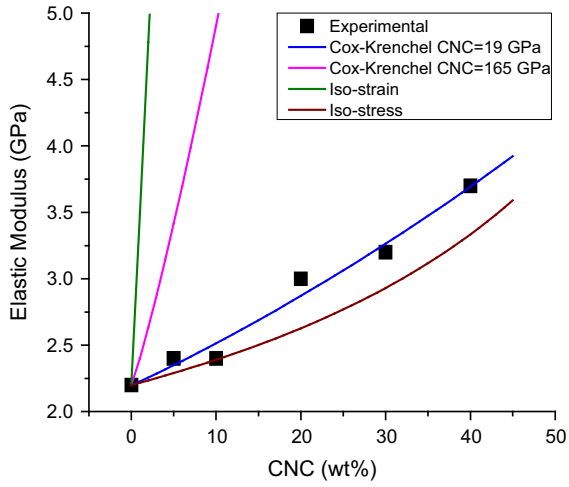

Fig. 7 Experimental elastic modulus and the Cox-Krenchel Model predictions for varying CNC elastic moduli. Also the predicted isostrain and isostress curves, with a CNC elastic modulus of 165 GPa

microscopy, suggests this may not be the dominate mechanism. In contrast, the PAN-co-MAA/CNC interface is most likely non-ideal so that the 100% efficient stress transfer assumed in the Cox-Krenchel model would be unrealistic, suggesting this may be a more dominate mechanism. In partial support for this, the calculated interfacial shear strength of 27 MPa (from Eq. 1) is low, and FTIR results showed there was no observable interaction between the CNC and the PAN, while there was interaction between the CNC and MAA, but the MAA only compromises of 4% of the polymer.

Comparing the results of the current study to the study by Chang et al. (2015) which studied the role of CNC additions to PAN-co-MAA/CNC fibers. The addition of 10 wt% CNC loading was shown to increase the elastic modulus of the neat fibers from 14.5 to 19.6 GPa, and the tensile strength from 624 to 709 MPa. These properties are considerably higher than the neat and composite films produced in the current study (see Table 1). While the same polymer and CNC were used, the differences in properties are considered to be associated with increases in CNC alignment, PAN-co-MAA polymer alignment, and in PAN-co-MAA crystallinity within the fiber as compared to the films, each of which have been shown to increase composite stiffness in the direction of alignment (Chen et al. 2014; Lai et al. 2011; Reising et al. 2012; Sehaqui et al. 2012). The larger increase in properties with the addition of CNC is likely due to the increase of PAN-co-MAA crystallinity with increasing CNC loading, and the highly aligned CNC, Herman's orientation factor of 0.9. While in contrast for the films used in the current study the PAN-co-MAA and CNC had a 2-D random orientation, with no change in crystallinity with the addition of CNC.

Conclusion

The addition of CNC to PAN-co-MAA was shown to alter the suspension rheology, and the thermal–mechanical properties of the corresponding composites. A solution of PAN-co-MAA and suspensions of PAN-co-MAA/CNC were made with a solid content of $\approx$4 wt%, with CNC loadings as high as 40 wt% of the solid content. The addition of CNC lead to suspensions with higher viscosities, and a shear thinning behavior as compared to the Newtonian behavior of neat PAN-co-MAA. Additionally, an aging effect was observed for all the PAN-co-MAA/CNC suspensions with the viscosities increasing over time, and is believed to result from time dependent polymer adsorption onto the CNC. Neat PAN-co-MAA and PAN-co-MAA/CNC films with up to 40 wt% CNC loading were produced by solution casting. These films were optically transparent, and maintained a similar level of transparency. The Tg increased from 92 °C for the neat polymer to 118 °C at 30 wt% CNC loading. Thermal stability of PAN-co-MAA/CNC was greater than both the neat PAN-co-MAA and neat CNC for temperatures under 350 °C in both air and nitrogen. Additionally, the residue yield of the composites was higher than predicted from rule-of-mixture. These thermal results indicate chemical interaction between the PAN-co-MAA and CNC when heated, which has yet to be identified. FTIR results show an interaction between the CNC and the carbonyl group of the MAA copolymerized with the PAN, but no observable interaction between the CNC and PAN. The addition of CNC did not change the degree of PAN-co-MAA crystallinity so the polymer matrix structure was maintained. There was a trend of increasing elastic modulus and tensile strength with increasing CNC loading. Comparing the neat PAN-co-MAA to the 40 wt% CNC loaded film, the elastic modulus increased from 2.2 to 3.7 GPa, the tensile strength increased from 75 to 132 MPa, while the strain a break decreased from 27.3 to 4.2%, respectively. The interfacial shear strength between the PAN-co-MAA and CNC was estimated to be 27 MPa, which is lower than the critical interfacial strength needed to fully utilize the tensile strength of the CNC. The storage modulus of PAN-co-MAA increased from 3.9 to 10.5 GPa at 40 wt% CNC loading at 35 °C.

Acknowledgments This work was financially supported by the Renewable Bioproducts Institute at Georgia Institute of Technology and by the Air Force Office of Scientific Research (Grant# FA9550-14-1-0194).

References

Aggour Y, Aziz M (2000) Degradation of polyacrylonitrile by low energy ion beam and UV radiation. Polym Test 19:261–267

Agustin MB, Ahmmad B, De Leon ERP, Buenaobra JL, Salazar JR, Hirose F (2013) Starch-based biocomposite films

reinforced with cellulose nanocrystals from garlic stalks. Polym Compos 34:1325–1332
Anderson BJ, Zukoski CF (2009) Rheology and microstructure of entangled polymer nanocomposite melts. Macromolecules 42:8370–8384
Bai H, Wang X, Zhou Y, Zhang L (2012) Preparation and characterization of poly (vinylidene fluoride) composite membranes blended with nano-crystalline cellulose. Prog Nat Sci Mater Int 22:250–257
Battegazzore D, Bocchini S, Frache A (2016) Thermomechanical improvement of glycerol plasticized maize starch with high loading of cellulose, flax and talc fillers. Polym Int 65:955–962
Bondeson D, Mathew A, Oksman K (2006) Optimization of the isolation of nanocrystals from microcrystalline cellulose by acid hydrolysis. Cellulose 13:171–180
Chang H, Chien A-T, Liu HC, Wang P-H, Newcomb BA, Kumar S (2015) Gel spinning of polyacrylonitrile/cellulose nanocrystal composite fibers. ACS Biomater Sci Eng 1:610–616
Chang H, Luo J, Bakhtiary Davijani AA, Chien A-T, Wang P-H, Liu HC, Kumar S (2016) Individually dispersed wood-based cellulose nanocrystals. ACS Appl Mater Interfaces 8:5768–5771
Chazeau L, Cavaille J, Perez J (2000) Plasticized PVC reinforced with cellulose whiskers. II. Plastic behavior. J Polym Sci Pol Phys 38:383–392
Chen H, Ding Y, Lapkin A (2009) Rheological behaviour of nanofluids containing tube/rod-like nanoparticles. Powder Technol 194:132–141
Chen S, Schueneman G, Pipes RB, Youngblood J, Moon RJ (2014) Effects of crystal orientation on cellulose nanocrystals–cellulose acetate nanocomposite fibers prepared by dry spinning. Biomacromolecules 15:3827–3835
Cho D, Yoon SB, Drzal T (2009) Cellulose-based natural fiber topography and the interfacial shear strength of henequen/unsaturated polyester composites: influence of water and alkali treatments. Compos Interfaces 16:769–779
Cox H (1952) The elasticity and strength of paper and other fibrous materials. Br J Appl Phys 3:72
Derakhshandeh B, Petekidis G, Sabet SS, Hamad WY, Hatzikiriakos SG (2013) Ageing, yielding, and rheology of nanocrystalline cellulose suspensions. J Rheol 57:131–148
Ebeling T, Paillet M, Borsali R, Diat O, Dufresne A, Cavaille J, Chanzy H (1999) Shear-induced orientation phenomena in suspensions of cellulose microcrystals, revealed by small angle X-ray scattering. Langmuir 15:6123–6126
Eichhorn SJ (2011) Cellulose nanowhiskers: promising materials for advanced applications. Soft Matter 7:303–315
Elazzouzi-Hafraoui S, Nishiyama Y, Putaux J-L, Heux L, Dubreuil F, Rochas C (2007) The shape and size distribution of crystalline nanoparticles prepared by acid hydrolysis of native cellulose. Biomacromolecules 9:57–65
Fortunati E, Puglia D, Monti M, Santulli C, Maniruzzaman M, Kenny JM (2013) Cellulose nanocrystals extracted from okra fibers in PVA nanocomposites. J Appl Polym Sci 128:3220–3230
Girouard N, Schueneman GT, Shofner ML, Meredith JC (2015) Exploiting colloidal interfaces to increase dispersion, performance, and pot-life in cellulose nanocrystal/waterborne epoxy composites. Polymer 68:111–121
Guo H, Minus ML, Jagannathan S, Kumar S (2010) Polyacrylonitrile/carbon nanotube composite films. ACS Appl Mater Interfaces 2:1331–1342
Habibi Y, Lucia LA, Rojas OJ (2010) Cellulose nanocrystals: chemistry, self-assembly, and applications. Chem Rev 110:3479–3500
Haspel B, Hoffmann C, Elsner P, Weidenmann K (2015) Characterization of the interfacial shear strength of glass-fiber reinforced polymers made from novel RTM processes. Int J Plast Technol 19:333–346
Huang S, Liu Z, Yin C, Wang Y, Gao Y, Chen C, Yang M (2011) Enhancement effect of filler network on isotactic polypropylene/carbon black composite melts. Colloid Polym Sci 289:1673–1681
Jiang L, Morelius E, Zhang J, Wolcott M, Holbery J (2008) Study of the poly (3-hydroxybutyrate-co-3-hydroxyvalerate)/cellulose nanowhisker composites prepared by solution casting and melt processing. J Compos Mater 42:2629–2645. doi:10.1177/0021998308096327
Kamal MR, Khoshkava V (2015) Effect of cellulose nanocrystals (CNC) on rheological and mechanical properties and crystallization behavior of PLA/CNC nanocomposites. Carbohyd Polym 123:105–114
Karpushkin E, Berkovich A, Artemov M, Sergeev V (2014) Rheological properties of polyacrylonitrile solutions containing highly dispersed carbon nanotubes. Polym Sci Ser A+(56):681–686
Kelly A, Tyson aW (1965) Tensile properties of fibre-reinforced metals: copper/tungsten and copper/molybdenum. J Mech Phys Solids 13:329–350
Khan A et al (2012) Mechanical and barrier properties of nanocrystalline cellulose reinforced chitosan based nanocomposite films. Carbohyd Polym 90:1601–1608
Kiziltas EE, Kiziltas A, Bollin SC, Gardner DJ (2015) Preparation and characterization of transparent PMMA–cellulose-based nanocomposites. Carbohyd Polym 127:381–389
Krenchel H (1964) Fibre reinforcement; theoretical and practical investigations of the elasticity and strength of fibre-reinforced materials. Dissertation, Technical University of Denmark
Kumar A, Negi YS, Choudhary V, Bhardwaj NK (2014) Characterization of cellulose nanocrystals produced by acid-hydrolysis from sugarcane bagasse as agro-waste. J Mater Phys Chem 2:1–8
Lai C et al (2011) Investigation of post-spinning stretching process on morphological, structural, and mechanical properties of electrospun polyacrylonitrile copolymer nanofibers. Polymer 52:519–528
Lee K-Y, Aitomäki Y, Berglund LA, Oksman K, Bismarck A (2014) On the use of nanocellulose as reinforcement in polymer matrix composites. Compos Sci Technol 105:15–27
Li Z, Young RJ, Wilson NR, Kinloch IA, Vallés C, Li Z (2016) Effect of the orientation of graphene-based nanoplatelets upon the Young's modulus of nanocomposites. Compos Sci Technol 123:125–133
Lin N, Dufresne A (2014) Nanocellulose in biomedicine: current status and future prospect. Eur Polym J 59:302–325
Lin N, Huang J, Chang PR, Feng J, Yu J (2011) Surface acetylation of cellulose nanocrystal and its reinforcing

function in poly (lactic acid). Carbohyd Polym 83:1834–1842
Liu JC, Martin DJ, Moon RJ, Youngblood JP (2015) Enhanced thermal stability of biomedical thermoplastic polyurethane with the addition of cellulose nanocrystals. J Appl Polym Sci 132:41970
Ljungberg N, Cavaillé J-Y, Heux L (2006) Nanocomposites of isotactic polypropylene reinforced with rod-like cellulose whiskers. Polymer 47:6285–6292
Loginova EV, Mikheev IV, Volkov DS, Proskurnin MA (2016) Quantification of copolymer composition (methyl acrylate and itaconic acid) in polyacrylonitrile carbon-fiber precursors by FTIR-spectroscopy. Anal Methods 8:371–380
Ma L, Zhang Y, Meng Y, Anusonti-Inthra P, Wang S (2015) Preparing cellulose nanocrystal/acrylonitrile-butadiene-styrene nanocomposites using the master-batch method. Carbohyd Polym 125:352–359
Maqsood HS, Baheti V, Wiener J, Militky J (2016) Reinforcement of enzyme hydrolyzed longer jute micro crystals in polylactic acid. Polym Composite. doi:10.1002/pc.24036
Marcovich N, Auad M, Bellesi N, Nutt S, Aranguren M (2006) Cellulose micro/nanocrystals reinforced polyurethane. J Mater Res 21:870–881
Moon RJ, Martini A, Nairn J, Simonsen J, Youngblood J (2011) Cellulose nanomaterials review: structure, properties and nanocomposites. Chem Soc Rev 40:3941–3994
Newcomb BA, Chae HG, Gulgunje PV, Gupta K, Liu Y, Tsentalovich DE, Pasquali M, Kumar S (2014) Stress transfer in polyacrylonitrile/carbon nanotube composite fibers. Polymer 55:2734–2743
Ozkul M, Mark J, Aubert J (1993) The elastic and plastic mechanical responses of microcellular foams. J Appl Polym Sci 48:767–774
Park S-J (2015) Carbon fibers, vol 210. Springer, Dordrecht
Rahaman MSA, Ismail AF, Mustafa A (2007) A review of heat treatment on polyacrylonitrile fiber. Polym Degrad Stabil 92:1421–1432
Reising AB, Moon RJ, Youngblood JP (2012) Effect of particle alignment on mechanical properties of neat cellulose nanocrystal films. J Sci Technol For Prod Process 2:32–41
Rescignano N, Fortunati E, Montesano S, Emiliani C, Kenny JM, Martino S, Armentano I (2014) PVA bio-nanocomposites: a new take-off using cellulose nanocrystals and PLGA nanoparticles. Carbohyd Polym 99:47–58
Roohani M, Habibi Y, Belgacem NM, Ebrahim G, Karimi AN, Dufresne A (2008) Cellulose whiskers reinforced polyvinyl alcohol copolymers nanocomposites. Eur Polym J 44:2489–2498
Schuster P (1969) LCAO–MO studies on hydrogen bonding: the interaction between carbonyl and hydroxyl groups. Int J Quantum Chem 3:851–871
Sehaqui H, Ezekiel Mushi N, Morimune S, Salajkova M, Nishino T, Berglund LA (2012) Cellulose nanofiber orientation in nanopaper and nanocomposites by cold drawing. ACS Appl Mater Interfaces 4:1043–1049
Siqueira G, Bras J, Dufresne A (2010) Cellulosic bionanocomposites: a review of preparation, properties and applications. Polymers 2:728–765
Swentek I, Wood J (2013) Using the lap-shear test to measure polymer composite interfacial strength. In: The 19th international conference on composite materials, proceedings, 2013
Thomason J, Vlug M, Schipper G, Krikor H (1996) Influence of fibre length and concentration on the properties of glass fibre-reinforced polypropylene: part 3. Strength and strain at failure. Compos Part A Appl S 27:1075–1084
Visakh P, Thomas S, Oksman K, Mathew AP (2012) Crosslinked natural rubber nanocomposites reinforced with cellulose whiskers isolated from bamboo waste: processing and mechanical/thermal properties. Compos Part A Appl S 43:735–741
Xu S, Girouard N, Schueneman G, Shofner ML, Meredith JC (2013a) Mechanical and thermal properties of waterborne epoxy composites containing cellulose nanocrystals. Polymer 54:6589–6598
Xu X, Yang Y-Q, Xing Y-Y, Yang J-F, Wang S-F (2013b) Properties of novel polyvinyl alcohol/cellulose nanocrystals/silver nanoparticles blend membranes. Carbohyd Polym 98:1573–1577
Yu H-Y, Qin Z-Y, Liu Y-N, Chen L, Liu N, Zhou Z (2012) Simultaneous improvement of mechanical properties and thermal stability of bacterial polyester by cellulose nanocrystals. Carbohyd Polym 89:971–978
Yu H-y, Qin Z-y, Zhe Z (2011) Cellulose nanocrystals as green fillers to improve crystallization and hydrophilic property of poly (3-hydroxybutyrate-co-3-hydroxyvalerate). Prog Nat Sci Mater Int 21:478–484
Zafeiropoulos NE (2011) Interface engineering of natural fibre composites for maximum performance. Woodhead Publishing, Sawston